Bio-inspired gust mitigation system for a flapping wing UAV: modeling and simulation

Article *in* Journal of the Brazilian Society of Mechanical Sciences and Engineering · November 2019

DOI: 10.1007/s40430-019-2044-9

2 authors:

Saddam Hussain Abbasi
Center For Advanced Studies In Engineering
16 PUBLICATIONS **78** CITATIONS
SEE PROFILE

Asif Mahmood Mughal
University of Arkansas at Little Rock
98 PUBLICATIONS **450** CITATIONS
SEE PROFILE

Journal of the Brazilian Society of Mechanical Sciences and Engineering (2019) 41:524
https://doi.org/10.1007/s40430-019-2044-9

TECHNICAL PAPER

Bio-inspired gust mitigation system for a flapping wing UAV: modeling and simulation

S. H. Abbasi[1] · A. Mahmood[1]

Received: 20 September 2018 / Accepted: 16 October 2019

Abstract

The growing use of drones today necessitates improved UAVs performance and capabilities. These requirements include flights in operational environments full of obstacles which present navigation and stability problems due to large-scale turbulence. To address this major concern, turbulence alleviation capabilities of natural counterparts have been studied in depth. Birds use inherent active and passive flow mechanism in their flapping wings and also deflection of covert feathers to stabilize themselves in turbulent airflows. This paper presents a novel bio-inspired gust mitigation system (GMS) for flapping wing UAVs mimicking covert feathers of birds. GMS senses the forces experienced from turbulent airflows and actuates to perform local airflow manipulations to alleviate them. GMS comprises of electromechanical feathers capable of deflecting out of the airfoil once they encounter turbulence. Modeling of single electromechanical feather assists in development of a complete GMS model that is further integrated in wing, modeled as flexible Euler–Bernoulli beam, and a complete dynamic model of flapping wing is obtained using bond graph modeling approach. We perform digital simulations and compute state-space equations to analyze model internal dynamics and responses. Comparison of the simulation results of wing without GMS and GMS-integrated wing, in response to vertical gust, confirms the efficacy of offered design. Furthermore, a good agreement between the present simulation results and experimental results from the literature validates the proposed model. As a result, the offered design successfully marks an initial step toward research into bio-inspired active gust mitigation systems for flapping wing UAVs.

Keywords Bio-inspiration · Gust mitigation system · Flapping wing UAV · Bond graph modeling

Abbreviations

GMS	Gust mitigation system
BGM	Bond graph model
GAS	Gust alleviation system
PZT	Piezoelectric transducer
EM	Electromechanical
UAV	Unmanned aerial vehicle
UAS	Unmanned aircraft system
CFD	Computational fluid dynamics
Sf	Source of flow
Se	Source of effort
MSf	Modulated source of flow
MSe	Modulated source of effort
TF	Transformer
GY	Gyrator
SJA	Synthetic jet actuators

1 Introduction

Flapping flight is one of the most effective modes of movement for majority of biological systems including birds and insects due to inherent aerodynamic advantages. Flyers exist in varying magnitudes of body size and flight speed [1], and flapping wings meet all the aerodynamic needs of locomotion in this wide range of scales. There is currently significant interest in developing miniature unmanned aerial systems, envisaged to perform a wide spectrum of missions. Many unmanned aerial vehicles (UAVs) including both fixed wing and flapping wing designs are increasingly common in

Technical Editor: Victor Juliano De Negri, D.Eng..

✉ S. H. Abbasi
abbasi882@gmail.com

A. Mahmood
amahmood1109@gmail.com

[1] Department of Electrical and Computer Engineering, Center for Advanced Studies in Engineering (CASE), Islamabad, Pakistan

Published online: 01 November 2019

daily life, such as selfie quadrotor, delivery drone, power line inspection flying robot and forest fire alarm unmanned flight vehicle [2–5]. However, turbulence has been a major factor of concern that applies limits to possible design options of all new airplanes [6]. It is evident as of now that the performance of current UAVs is still inferior to natural counterparts, and thus, insects and birds offer inspiration for the design of aerial robots with adequate aerial prowess.

A lot of research has been carried out into flapping wing performance; however, these results may not be applicable to flapping wing flight in natural environments. Almost all studies on flapping flight have been performed in quiescent or smooth wind conditions [7, 8]. This does not depict the aerial environment that flapping wing UAVs are likely to encounter outdoors. UAVs typically fly within the atmospheric boundary layer, a region that is optimum for UAV applications in Intelligence, Surveillance, and Reconnaissance (ISR) missions. The atmospheric boundary layer exists from the ground up to 400–1000 m and is highly turbulent [9]. The turbulent flows within this region, having towns and forests, are generated when the wind interacts with buildings or trees, and consequently, vortices and regions of high turbulence are generated as shown in Fig. 1 [10–12].

In the presence of wind gusts and high turbulence, the performance of UAVs can deteriorate significantly [13]. Research in [14] presents turbulent flight environment close to the ground and its effects on fixed and flapping wing UAVs. The study in [15] declares turbulence as a major factor for the loss of various UAVs. This loss is due to lack of sensory feedback to the pilot, who resultantly could not detect changes in flight condition due to the incomplete data presented on the screens.

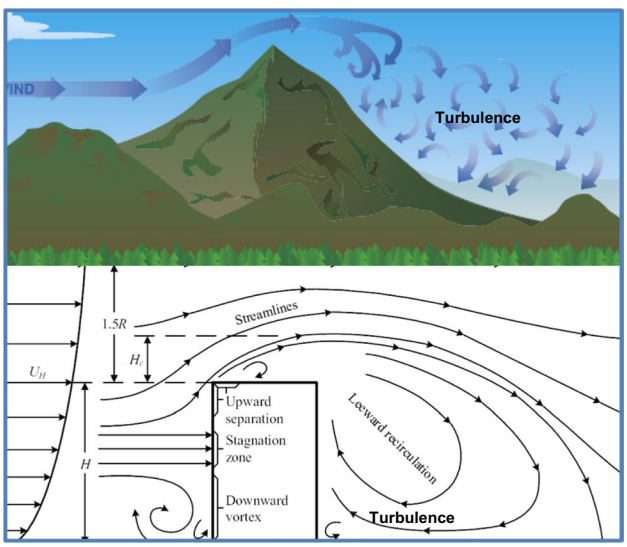

Fig. 1 Airflow around mountains and buildings [11]

To address this serious concern of turbulence, limiting possible design options of UAVs, several efforts have been made to date. The first ever gust alleviation system (GAS) in the literature was presented in 1914 for a "stabilizing device for flying machines" [16]. Since then, many efforts have been made to design an autonomous GAS, including work performed by the Bristol Aeroplane Company 1949 [17], Douglas Corporation 1950 [18] and NACA 1952 [19]. Each system design was declared unfit even before their first journey [20].

Modern UAV designs mostly need effective sensors that can rapidly detect turbulence-induced motion perturbations. Existing UAV attitude control systems rely on inertial sensors. These systems can be described as reactive; detecting the disturbance only after the aircraft has responded to the disturbing phenomena. Researchers in [21] have reviewed state-of-the-art reactive attitude sensing techniques. They found that the use of single sensors is insufficient for flight control in the presence of turbulence and that potential gains can be realized from multi-sensor systems. Another research [22] proves that current conventional reactive attitude sensors lack the necessary response times for attitude control in high-turbulence environments. Therefore, they are presented in greater detail novel and emerging biologically inspired sensors, which can sense the disturbances before a perturbation is induced. Bio-inspired flow and pressure-based sensors were found to be the most promising for complementing or replacing current inertial-based reactive attitude sensors. However, application of these bio-inspired sensors to alleviate turbulence for flapping wing UAVs is yet to be studied.

Study in [23] proposed sensor-based gust perturbation alleviation control method using real-time pressure sensor. Pressure measurement in this research provides phase-advance information on external disturbance, which the conventional inertial measurement cannot. The estimated rolling moment from two sensors is incorporated into a traditional flight controller that generates commands to mitigate it. This study is confined only for fixed wing flights, and its advantages for flapping wing flights need to be explored.

Blower and Wickenheiser in [24] have presented a biologically inspired variant of flow sensors that come in the form of feather-like wing panels. They replicate concept of avian primary and secondary feathers in fixed wing UAVs and explore their use for gust alleviation. The underlying concept is to integrate sensors with aerodynamic surfaces for flow control and to detect and alleviate gusts. Additionally, trajectory deviation is also expected to reduce considerably, allowing air-to-air refueling of UAS, which requires high maneuverability. This approach mimics avian primary and secondary feathers' splaying mechanism to mitigate turbulence and has been presented for fixed wing UAVs only.

Synthetic jet by active flow control is another technique for gust alleviation. These jets when integrated into the

wing extend the flight envelope of the aircraft to higher angles of attack, thus reducing the potential for wing stall during aggressive maneuvers. Barron Associates have researched that synthetic jets generate an oscillating flow upon the wing's surface [25]. By generating this airflow, the boundary layer can remain attached in more extreme conditions, thus enabling the aircraft to remain stable in turbulent air flows. The application of SJAs to an active gust alleviation system is yet to be realized. Furthermore, designing for small-scale flapping wing UAVs is required to be done.

Many techniques have been utilized to obtain turbulence data in the atmospheric boundary layer. Some of them include sonic detection and ranging (SODAR) and light detection and ranging (LIDAR) sensors. SODAR and LIDAR are used to profile the velocity field by emitting and measuring the scatter of sound and light, respectively. The system actuates control surfaces in response to the readings to alleviate the incoming turbulent airflow [26]. However, SODAR- and LIDAR-based gust mitigation programs till today have not been applied into smaller UAVs due to space and weight limitations.

Vortex generator is another technique that has been integrated onto numerous aircraft. This device generates micro-vortices over the surface of wing that prevents boundary layer separation. While the aircraft is operating within bodies of air that have high eddy dissipation rates [27], the vortex generators delay flow separation by drawing highly energized free-stream fluid into the boundary layer, which consequently delays wing stall [28]. Exploration of vortex generator utilization to small-scale fixed and flapping wing drones is still in budding stages.

The in-depth study of avian flight has revealed that turning radius, roll rates and stability is achieved by using their adaptive wing structures to achieve nearly instantaneous adjustments required to maintain their flight path through a wide range of environments and weather conditions. During high turbulence and gusts, one of the techniques birds adopt is an intermittent flight (non-flapping phase) in which birds extend their wings and glide or hover. The covert feathers present beside primary feathers during these intermittent flights get activated to mitigate turbulence and gusts as shown in Fig. 2 [29].

The evident gap in the research of active gust alleviation systems for flapping wing UAVs form the basis for this paper that gets the motivation from birds and presents a novel design of covert feathers inspired distributed gust mitigation system (GMS) for flapping wing UAVs. GMS comprises of electromechanical (EM) feathers that are incorporated in flapping wing. GMS actuates only during intermittent flights to mitigate gust just like covert feathers of birds. During all other times, it remains integrated with overall wing to maintain airfoil in overall profile. It offers multiple potential flight benefits, including increased maneuverability and stability in unknown flow environments.

Fig. 2 Covert feathers deflect in response to gusts [29]

First, we present a block diagram of a single EM feather to give an overview of its working methodology. The block diagram leads to the model of single EM feather with detail analytical understanding. Further, we develop model of a complete GMS comprising of 16 EM feathers. Then, we integrate this GMS in flapping wing that we model as flexible Euler–Bernoulli beam and formulate a complete dynamic model of a gust mitigating flapping wing. We use bond graph modeling approach for detailed model and for the digital simulation of flapping wing using 20-sim software. Furthermore, we compute state-space equations to analyze model internal dynamics and responses. Finally, we simulate the model to confirm its efficacy and compare the results with experimental studies in the literature in order to validate the proposed scheme.

2 Bio-inspired GMS design

We develop GMS for small flapping wing UAVs. The prototype under investigation is based upon Festo Smart Bird [30]. The smart bird has a wing span of 2 m and mean chord length of 0.25 m. The GMS comprises of 16 biomimetic EM feathers out of which 8 are integrated in the wings upper surface and 8 are installed on wings lower surface at the location where covert feathers of avian are present as shown in Fig. 3. The size of GMS is 12×6 in. Single EM feather comprises of a flap, mechanical linkage, linear encoder, piezoelectric transducer (PZT), voice coil, amplifier and controller. The PZTs due to small size and multi-functionality are used in feathers keeping in view the size limitations of wings. Furthermore, PZTs can simultaneously act as sensors and actuators.

The flapping wing has a skeletal design comprising of spars and ribs to bear load. The GMS design allows wing to maintain the airfoils profile during flapping flights as EM feathers remain tightly attached to the wing. GMS actuates only during high turbulence once UAV adapts to intermittent

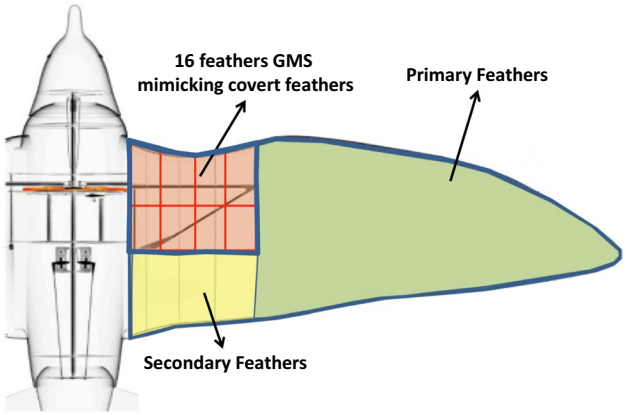

Fig. 3 Location of a proposed GMS in flapping wing [30]

flight, and as a result EM feathers deflect out of the airfoil to allow vertical gusts to pass through the wing. Resultantly, the cross-sectional wing area that experiences gust is significantly reduced. The deflection angle of feathers is directly proportional to the amount of gust experienced as shown in Fig. 4.

Figure 5 shows the detailed component diagram of the EM feather. The rotational motion of flap in response to incident vertical gust is converted into axial force that is applied to PZT through mechanical linkage and linear encoder. The PZT generates a voltage equivalent to the magnitude of gust force experienced and feeds it to a local controller which further uses it to generate desired control input. This command from the controller in the form of current is fed to a voice coil. Shaft inside the voice coil now acts as a current carrying conductor inside a magnetic field. Resultantly, the shaft moves out with certain force that is applied to the flap through mechanical linkage for final deflection. Therefore, the gust passes through the feathers with minimum interaction with the cross-sectional area of wing.

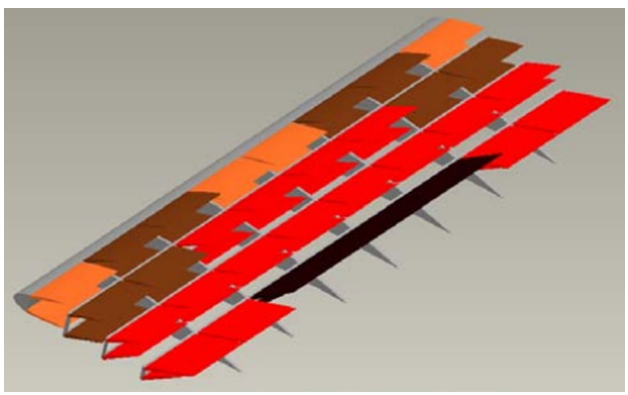

Fig. 4 Cross-sectional wing area reduction due to covert feather's deflection in response to varying gust speed [24]

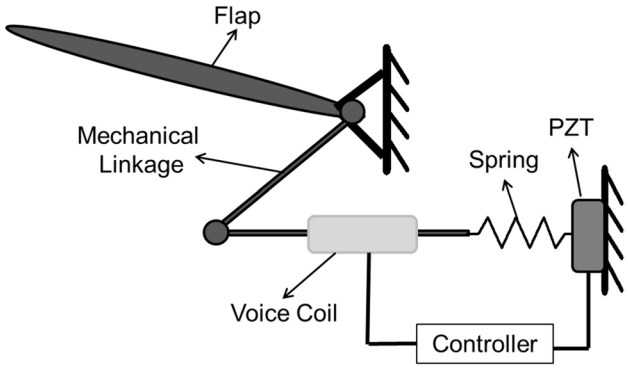

Fig. 5 Electromechanical feather

Each EM feather is a closed-loop feedback system. The GMS is independent of the centralized flight control system. The proposed design allows localized analysis of data reducing reaction times as compared to existing gust alleviation systems having delayed response times. The counteractive force generated by each EM feather is equivalent to the gust intensity it experiences. During larger gusts, multiple numbers of feathers are actuated since singular feather is not enough to counteract the turbulence. Consequently, GMS offers distributed hierarchal response generation capability of EM feathers minimizing stress and load on single feather as gust is distributed over a region of the wing rather than a singular point.

3 Modeling framework

Modeling is the process of representing a system in the form of a model which includes its construction and working. This model is similar to a real system, which helps to analyze and predict the effect of changes to the system. Simulation of a system is the operation of a model in terms of time or space, which assists to examine the performance of an existing or a proposed system. [31].

Bond graph modeling technique is used in this research which is a well-developed tool to deal with multi-energy domain systems with graphical and mathematical representations. This method offers a powerful tool to develop dynamic models of numerous systems including electrical, mechanical, magnetic, hydraulic and thermal, or any combinations of these. Dynamic analysis based on the bond graph concept is carried out to define certain basic elements including resistance, inductance, capacitance, sources of flow and effort, junctions, gyrators and transformers. Assigning appropriate causality to the bonds helps to derive the differential equations of the system. Consequently, application of bond graphs to multi-body dynamic systems considerably reduces the efforts required to model multi-domain systems [32].

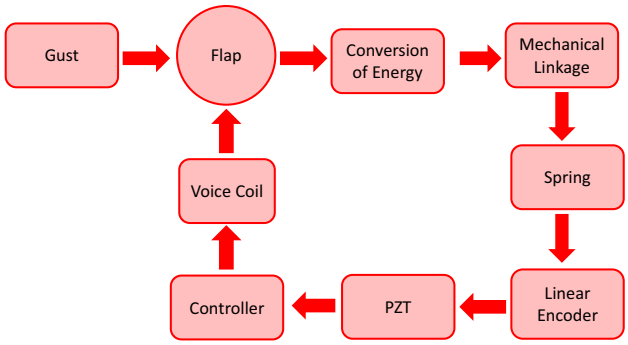

Fig. 6 Block diagram of a single EM feather

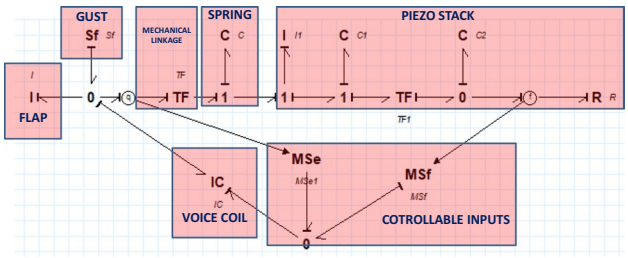

Fig. 7 BGM of a single EM feather

3.1 Model of a single EM feather

Before we develop detailed bond graph model (BGM) of bio-inspired GMS, we present main working of single EM feather through a block diagram in Fig. 6.

The block diagram in Fig. 6 further disseminates into a detailed BGM of a single EM feather. Figure 7 shows the graphical representation of single EM feather in the form of dynamic bond graph model obtained through 20-sim software. There are 8 energy-storing elements making the eighth-order model of the system. There are three inputs Sf (source of flow), MSe (modulated source of effort) and MSf (modulated source of flow), which are components of input vector $\vec{u}(t)$. Gust is the disturbance input represented as Sf, whereas MSe (force applied on mechanical linkage) and MSf (current input to voice coil) are the controllable inputs.

The BGM obtained is used to formulate state-space equations given as Eqs. (1)–(8). The state variables comprise of generalized momentum p_1, p_2, p_3 at every inertia element and generalized displacement q_1, q_2, q_3, q_4 at every compliance element. State variable q_5 is the state of displacement sensor used in the bond graph.

$$\dot{p}_1 = ic \cdot p_3 + ic \cdot q_3 \tag{1}$$

$$\dot{q}_1 = \frac{1}{I_1} \cdot p_2 \tag{2}$$

$$\dot{p}_2 = \frac{ic}{l} p_3 + \frac{ic}{l} q_3 - \frac{1}{C} q_1 - \frac{1}{C_1} q_2 - \frac{m}{C_2} q_4 \tag{3}$$

$$\dot{q}_2 = \frac{1}{I_1} \cdot p_2 \tag{4}$$

$$\dot{p}_3 = q_5 \tag{5}$$

$$\dot{q}_3 = S_f - \frac{1}{l \cdot I_1} p_2 - \frac{1}{I} p_1 \tag{6}$$

$$\dot{q}_4 = \frac{m}{I_1} p_2 - \frac{R}{C_2} q_4 \tag{7}$$

$$\dot{q}_5 = \frac{1}{l \cdot I_1} p_2 \tag{8}$$

3.2 Elastic wing model

In this section, we approximate the dynamic characteristics of the wing as an elastic beam in transverse vibration pivoted at one end. In the proposed model, we measure mass and elasticity as distributed parameters. Two methods generally used for modeling the distributed system include finite lumping and modal analysis. For the finite lumping method, a great number of reticulations are must for accurate low frequency response. However, this increase in the reticulations yields inaccuracies in higher frequencies as well as increase in the number of states. Hence, we use the modal approach to generate the bond graph model of our system, which is more accurate and flexible enough to be combined in the overall system model. The implementation of boundary conditions is also easy in modular approach [33].

The modal approach although is accurate; however, the transformer for modal contributions necessitates to be formed separately for several boundary conditions. Due to this reason, extension to the overall system model is not so simple. We integrate structural damping, which is normally small, by adding R elements to the 1-junctions showing motions of lumped or modal masses. Further, we attain the damping of rotational motions in the Euler–Bernoulli model by attaching a C-1-R module to the 0-junctions in which C elements signify flexural stiffness [34].

Furthermore, we model the flapping wing using Euler–Bernoulli beam as flexible element having pinned-free boundary conditions. Using Euler–Bernoulli beam, natural frequencies along with their modes used in the simulation can be analytically found. Moreover, the elastic flapping wing equation of motion using the Euler–Bernoulli elastic beam is to be integrated with aerodynamics and mass inertia loadings. Consequently, this beam can be used as a good alternate for a real elastic wing [35]. Figure 8 illustrates the

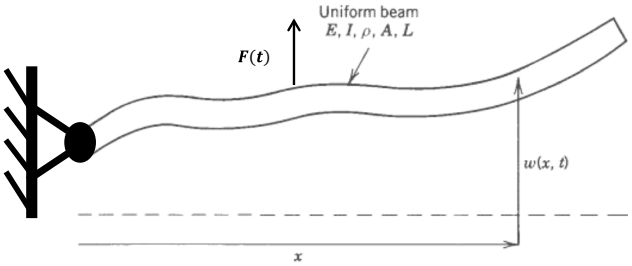

Fig. 8 Euler–Bernoulli Beam [34]

Euler–Bernoulli beam subjected to an external gust force F with respect to the hinge point.

The equation of motion of the elastic wing under transverse vibration due to external force is as follows [36]:

$$EI\frac{\partial^4 w}{\partial x^4} + \rho A\frac{\partial^2 w}{\partial t^4} = F\delta\left(x - x_1\right) \tag{9}$$

where EI, ρ, A and w are flexural rigidity, material density, cross-sectional area and deflection of the wing, respectively. The bending moments corresponding to the pivoted end are zero. Likewise, the shear force and bending moment associated with the free end are also zero. The mode shapes and frequency equation for pinned-free boundary conditions can be described as follows [36]:

$$\tanh \beta_n l - \tan \beta_n l = 0 \tag{10}$$

$$Y_n(x) = \left(\sinh \beta_n l + \sin \beta_n l\right)\left(\cosh \beta_n x + \cos \beta_n x\right) - \left(\cosh \beta_n l + \cos \beta_n l\right)\left(\sinh \beta_n x + \sin \beta_n x\right) \tag{11}$$

and $\beta_n l$ can be described as:

$$\beta_1 l = 3.92, \quad \beta_2 l = 7.06, \quad \beta_3 l = 10.2,$$

$$\beta_4 l = 13.35, \quad \beta l = 0 \text{ for rigid body} \tag{12}$$

where β_n represent the modal stiffness. Figure 9 shows the valid bond graph model of the elastic wing with one rigid mode and multiple flexible modes taken from [37]. This bond graph is obtained from modal Eq. (11) for $n = 1, 2, 3,\ldots$ The external force F (gust) stimulates each mode in accordance with Eq. (9). The transformers shown are simply the mode shapes from Eq. (11). Pinned-free boundary conditions resulted in one rigid mode and n elastic modes and are displayed in the bond graph. It is evident that the transformer elements attached to the rigid body mode apply the moment to these elements [37].

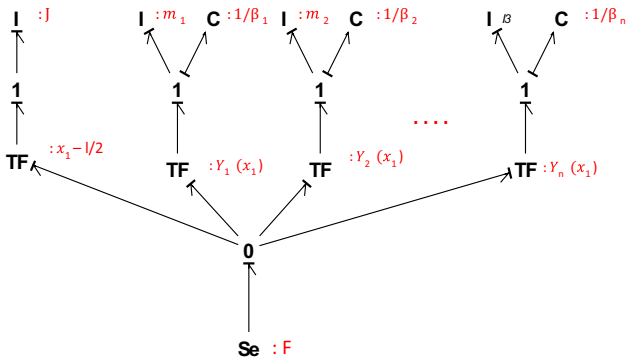

Fig. 9 BGM of an elastic wing [37]

3.3 Dynamic model of a complete flapping wing with GMS

Modeling of a single EM feather and elastic wing enables us to present bond graph model (BGM) of a GMS-installed flapping wing with ease. However, prior to that, we present main working of a complete flapping wing with GMS through a block diagram in Fig. 10. Input from the piezoelectric transducers (PZTs) depicting the amount of vertical gust incident on the feather is fed to a GMS controller for generation of desired control output for final deflection of flap. Figure 11 presents the BGM of a complete flapping wing with GMS installed in it. It is obtained by integrating BGM of GMS with the BGM of an elastic wing using a transformer.

There are 134 energy-storing elements making 134th-order model of the system. There are 16 disturbance inputs in the form of vertical gust applied to each feather, each shown as a source of flow (Sf–Sf15), which are components of input vector $\vec{u}(t)$. In addition, the disturbance in the form of gust is also applied to elastic wing as a source of flow (Sf) at 0 junction. There are a total of 32 controllable inputs, 16 of them are shown as modulated source of flow (MSf), and 16 are shown as modulated source of effort (MSe). From this bond graph model, we obtain state-space equations of the system. The state vector $\vec{x}(t)$ constitutes due to the generalized momentum at every inertia element and generalized displacement at every compliance element where there are only integral causalities. The resulting state matrix A is of

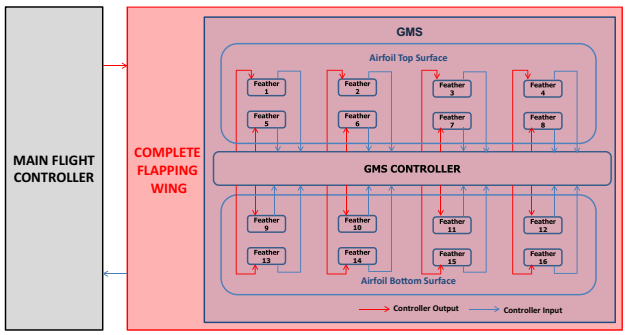

Fig. 10 Block diagram of flapping wing with GMS

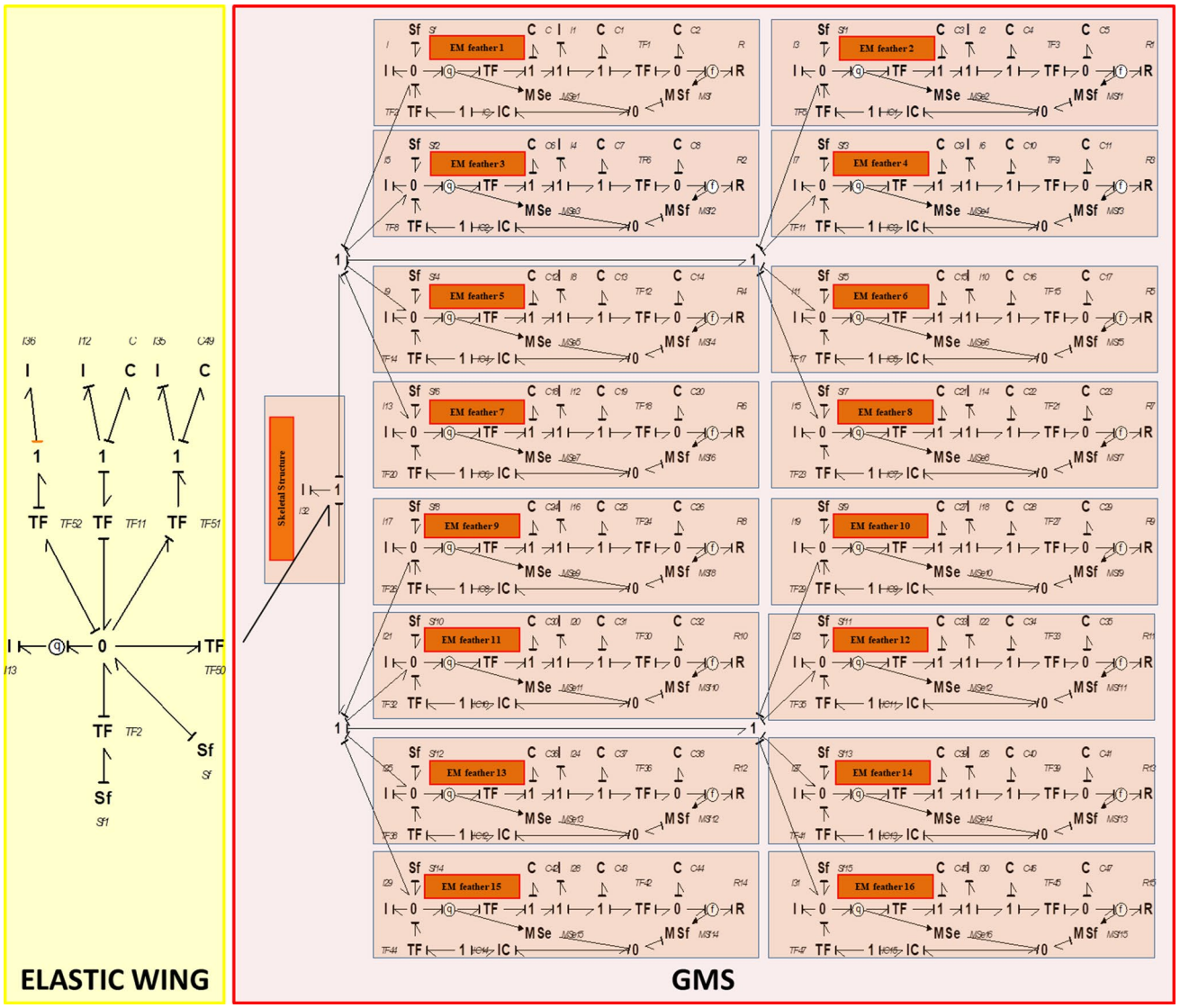

Fig. 11 BGM of a complete flapping wing with GMS

134 × 134 order, the input gain matrix B is of 134 × 16 order, and output gain matrix C is of 16 × 134 order.

4 Modeling of aerodynamic forces

The aerodynamic model of UAVs is generally created with a rigid wing [37]; however, despite complexity, the flexibility of the wing has been integrated. In flapping wing modeling, the effect of aerodynamics on the wing can be neglected since aerodynamic forces have smaller effect than inertial forces. Similarly, the study of wing flexibility reveals that the main wing bending is not due to the interaction between aeroelasticity and fluid but caused by inertia due to the wing mass distribution [38]. Assessment and calculation of aerodynamic and inertial forces on wings are investigable. If aerodynamic forces are vital to study the wing dynamics, wing bending needs to be predicted during each time step by computing the generated aerodynamic forces, and this is very time-consuming and challenging work [39].

We limit the scope of current study to simply simulate the aerodynamic lift in response to vertical gust. Consequently, we add this effect as a source of flow (Sf) term in the bond graph model. Further, we apply this force to elastic wing (with and without GMS) to analyze corresponding movement in z direction. This means that the motion of elastic wing is transformed to a continuous motion of a rigid body in the vertical direction using the MTF (modulated transformer) as shown in Fig. 11.

The complete modeling of the GMS-integrated flapping wing by incorporating all aerodynamic and structural

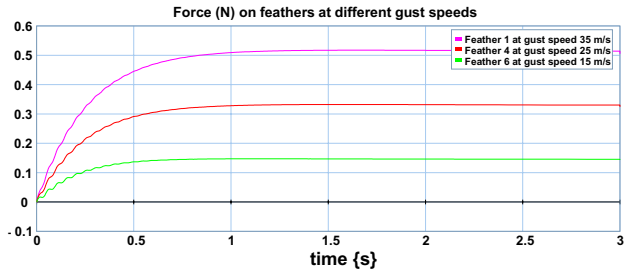

Fig. 12 Force on flaps from controller in response to vertical gust

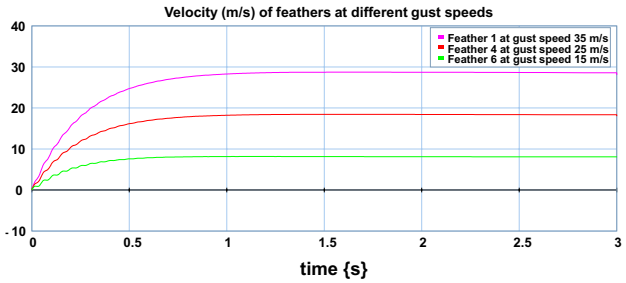

Fig. 13 Speed of flaps in response to vertical gust

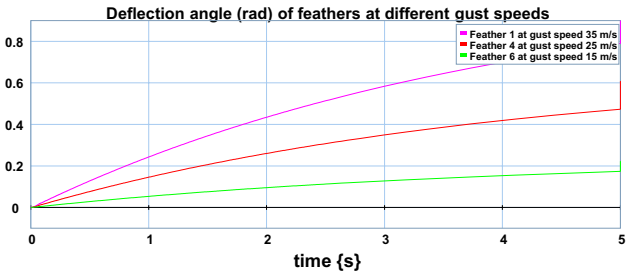

Fig. 14 Deflection angle of flaps in response to vertical gust

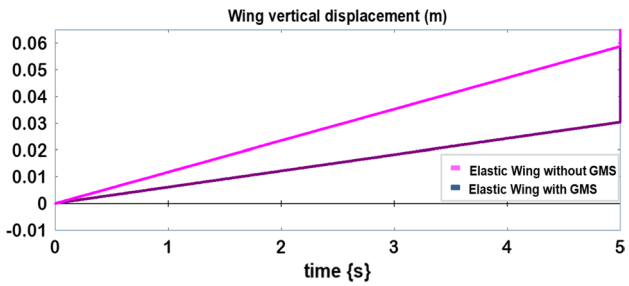

Fig. 15 Vertical displacement of wing (with and without GMS) in response to 25 m/s vertical gust

elements is complicated. To simplify the process, we make certain assumptions, such as ignoring a wide range of aerodynamic forces involved in flapping flights presented in recent studies [40] such as drag, thrust, wing wake, added mass, rotational inertia and rotational circulation. Furthermore, we approximate flapping wings as Euler–Bernoulli beams. In order to have a more realistic model that closely mimics natural counterparts, extension in work is needed. Adding certain new boundary conditions, extra degrees of freedoms, various input forces and moments and, moreover, altering the vibration modes of the wings need to be considered.

5 Results and discussions

Each of the 16 EM feathers in GMS configuration is in modular scheme from input to output. There are similar elements from each source of flow (Sf) till feather inertia (*I*) at the end with same parametric values. A skeletal structure consisting of ribs and bars is connected to all feathers as an inertia element (*I*32) adding an order to the overall system. We simulate the model by incidence of three different vertical gust intensities (35 m/s, 25 m/s, 15 m/s) at three different feathers (feather 1, feather 4 and feather 6). Figure 12 shows the force acting on flaps of these EM feathers by the voice coil. The voice coil actuates by GMS controller command in response to incident vertical gust intensities. Figure 13 shows the speed of these three flaps, and Fig. 14 shows the angle to which each of these flaps deflects out of the airfoil.

All of these figures clearly depict that the response of GMS is in desired range and is exactly proportional to the incident vertical gust intensity. The feather that experiences the maximum amplitude of gust receives maximum force from the controller and thus rotates at the maximum angle and vice versa. This validates the distributed hierarchal response generation capability of GMS minimizing stress and load on single feather.

In order to validate the effectiveness and accuracy of proposed GMS design, we apply vertical gust of 25 m/s as a source of flow (Sf*)* acting as a disturbance on an elastic wing model without GMS, presented in Fig. 9. Afterward, we apply the same vertical gust to an elastic wing model with GMS installed in it, presented in Fig. 11, and carryout dynamic simulations. The vertical displacement occurring in both the wings as a result of lift force generated by gust is shown in Fig. 15.

It is evident that the wing model having GMS installed in it has successfully mitigated the turbulence incident on it to 50% due to effective local air flow manipulations by independent feathers and has vertically displaced to only 0.03 m as compared to 0.06 m for the wing model without GMS. This numerical simulation validates the efficacy and accuracy of proposed model.

Table 1 shows a comparison between the results obtained by the present research and the experimental study carried out by [41]. Force on the wing in response to different wind

Table 1 Comparison between the results obtained by the present simulation and the experimental study at the same gust speed of 25 m/s

	Force (*N*)	Wing vertical displacement (*m*)
Present work		
Without GMS	8.1	0.06
With GMS	4	0.03
Experimental [41]	8.3	0.068

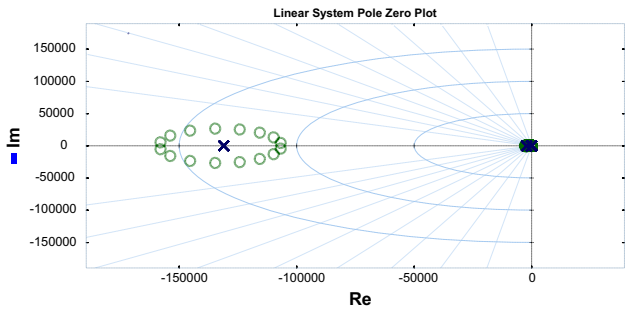

Fig. 16 Pole-zero plot of the linearized model

speeds (20 m/s, 25 m/s, 30 m/s) and corresponding vertical displacement of the wing is calculated using aerodynamic analysis on XFLR5 and structural analysis on CATIA V5, and the result is validated through wind tunnel experimentation [41]. Very good agreement between the simulation results of elastic wing (with and without GMS) at 25 m/s gust speed that were obtain in present work and experimental data confirms the validity and accuracy of the proposed model.

Electromechanical feather no 2 is taken as a case study for simplicity to understand system internal dynamics. Gust on flap (Sf1) is taken as input terminal, and final force acting on flap (I_3) is taken as output terminal. Linearization for this input–output in 20-sim provides 134th-order model in state space of transfer function realization. Figure 16 shows the pole-zero map of the linearized model which shows that all eigenvalues (poles) are internally stable. Gain and phase margins of the model with respect to input gust and output feather rotation in Fig. 17 show damping characteristics of the model in Bode plot. The step response of the same model in Fig. 18 shows again the stable characteristic from input to output. It must be noted that due to the similarity in modeling of all 16 feathers, responses of other feathers are also similar with differences in magnitude. These simulation results render output values exactly in the desired range and further depict the stable internal dynamics of system model validating the proposed model. The values and specifications of components for all 16 feathers are the same as that of one feather and are shown in Table 2 taken from [42].

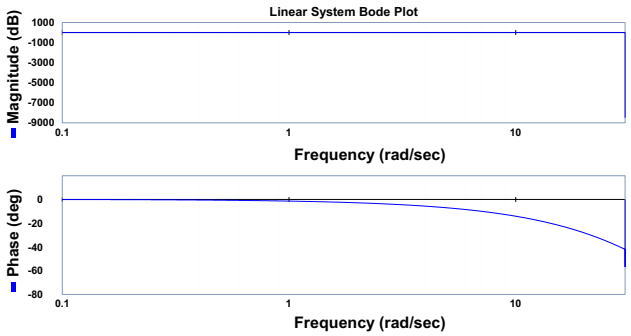

Fig. 17 Bode plot of the linearized system model

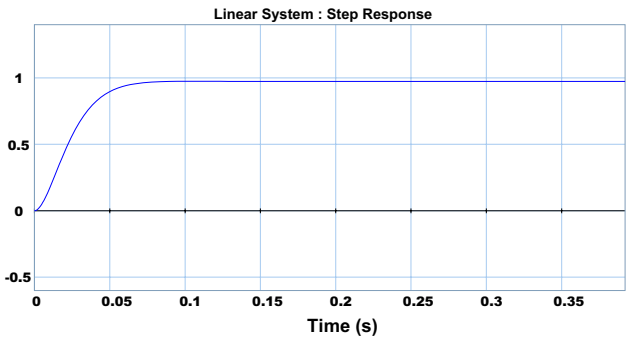

Fig. 18 Step response of the linearized model

6 Conclusion and future work

In this paper, we present literature review of existing turbulence alleviation systems along with their advantages and limitations. Void space in the area of flapping wing UAVs' capability to counter turbulent airflows necessitates detailed study of their natural counterparts. We present a novel bio-inspired gust mitigation system (GMS) design for flapping wing UAVs based on inspiration from birds' covert feathers. The installation of electromechanical (EM) feathers upon the wing surfaces of flapping wing UAVs minimizes the gusting forces experienced by the fuselage and payload. Each feather is a standalone unit that has its own microcontroller to allow localized data collection and analysis, thus reducing the system's response time. We develop bond graph model (BGM) of a bio-inspired EM feather using 20-sim. It leads to the development of BGM of a complete GMS comprising of 16 EM feathers. We further integrate the GMS model with validated elastic Euler–Bernoulli beam flapping wing model, taken from the literature and obtain a complete dynamic model of a flapping wing using bond graph modeling approach.

We simulate three different EM feathers (1, 4 and 6) using 20-sim at varying vertical gust intensities (35 m/s,

Table 2 Parameters of the system model

Element	Domain	Description	Value
Elastic wing			
I12, I35, I36	Mechanical	Modal mass	0.25 kg
C, C49	Mechanical	Modal stiffness	0.05 KN/m
TF 11, TF51, TF52	Mechanical	Modulus of transformer	0.07
I13	Mechanical	Mass moment of inertia	0.0024 Kgm^2
TF2	Mechanical	Modulus of transformer	0.1
GMS			
Flap			
I	Mechanical	Mass of flap	0.018 kg
I32	Mechanical	Mass of skeletal structure	0.098 kg
Sf	Mechanical	Gust velocity on flap	25 m/s
Voice coil actuator			
IC	Electrical	Inductance	0.89 H
	Mechanical	Stiffness	0.589 KN/m
Piezoelectric stack			
R	Electrical	Resistance between amplifier and PZT	5 Ω
I1	Mechanical	Mass of Stack	0.008 kg
C1	Mechanical	PZT spring stiffness	0.024 kN/m
C2	Electrical	PZT equivalent capacitance	1.5×10^{-7} F
TF1	Electrical	Electromechanical Coupling Ratio	0.478
Spring			
C	Mechanical	Stiffness of spring	0.03kN/m
Mechanical linkage			
TF	Mechanical	Transformer Ratio	0.2

25 m/s, 15 m/s). The corresponding force on flaps of these EM feathers generated through GMS controller is 0.51 N, 0.32 N and 0.14 N which deflects them out of the airfoil at 0.78 rad, 0.47 rad and 0.19 rad at the velocity of 29 m/s, 18 m/s and 8 m/s, respectively. These feathers splaying with varying force, velocity and at varying angles dependent on the amount of turbulent force experienced by the sensing feather validate the distributed hierarchal response capability of GMS minimizing stress and load on single feather by distributing gust over a region of the wing rather than a singular point.

Further, we linearize the model taking EM feather no 2 as a use case with vertical gust on it (Sf1) as input terminal and final force acting on its flap (I_3) as output terminal. We simulate and compute state-space equations to analyze model internal dynamics and responses. The pole-zero plot of the linearized model clearly depicts all 134 poles, both real and conjugate pairs, in left half plane, and the step response shows stable characteristics of the system model. The rise time of the step response is 0.05 s, settling time is 0.08 s, and steady state is 0.98 N, respectively. The step characteristics show values that are in desired range further reinforcing proposed model correctness.

Finally, the simulation results depict successful mitigation of gust up to 50% by GMS-installed flapping wing as compared to flapping wing without GMS as it vertically displaces to 0.03 m compared to 0.06 m in response to vertical gust of 25 m/s, thus validating the efficacy and accuracy of proposed model. Furthermore, very good agreement between the simulation results of elastic wing presented in present work and experimental data from the literature at same gust speed validates the proposed model.

Since current work is the first step toward design of an active gust mitigation system for flapping wing UAVs inspiring from birds and a step further from previous study by authors [42], we made certain assumptions to ease the progression, such as ignoring aerodynamic forces (drag, thrust, wing wake, added mass, rotational inertia and rotational circulation), considering wings as Euler–Bernoulli beams and mechanism of in-plane motion. In future, we plan to extend our work for modeling of a complete multi-body flapping wing UAV comprising of main body, accessories, flapping mechanism, fuselage, propulsion system along with incorporation of GMS in both flapping wings. Also, CFD modeling of the proposed design will be carried out for further in-depth study of aerodynamics of flapping flight as this research has only been confined to vertical aerodynamic forces (lift). Further, various control schemes including robust and optimal controls will be studied to minimize settling time and improve stability of the multi-body model.

Finally, physical design on the basis of proposed model will be carried out to endeavor a worthwhile addition of gust mitigation capability into flapping flight drones.

References

1. Ellington CP (1984) The aerodynamics of hovering insect flight: II. Morphological parameters. Phil Trans R Soc B 305:17–40
2. Rob M (2018) The autonomous selfie drone. https://www.news.mit.edu/2018/startup-skydio-autonomous-selfie-drone-0313. Assessed 25 July 2018
3. Anne G, Jordan T (2018) Delivery by drone: an evaluation of unmanned aerial vehicle technology in reducing CO_2 emissions in the delivery service industry. Transp Res Part D Transp Environ 61:58–67
4. Muhammad AG, Kundan K, Javed MA (2018) High-voltage transmission line inspection robot. In: International conference on engineering and emerging technologies (ICEET)
5. Zhang L, Wang B, Peng W, Li C, Zeping L, Guo Y (2015) A method for forest fire detection using UAV. Adv Sci Technol Lett 81:69–74
6. Advisory Group for Aerospace Research & Development (1986) Gust load prediction and alleviation on a fighter aircraft. AGARD, Report R-728
7. Grand C, Martinelli P, Mouret J-B, Doncieux S (2008) Flapping-wing mechanism for a bird-sized UAVS: design, modeling and control. In: 11th International symposium on advances in robot kinematics, France, pp 127–136
8. Jahanbin Z, Karimian S (2018) Modeling and parametric study of a flexible flapping-wing MAV using the bond graph approach. J Braz Soc Mech Sci Eng 40(2):96
9. NRG Travel. The Matterhorn, Switzerland. https://www.nrgtravel.com. Assessed 3 Aug 2018
10. Cionco RM, Vaucher GT, D'Arcy S, Bustillos M (2006) Near-building turbulent intensities, fluxes, and vortices. US Army Research Laboratory, Report J6.4
11. Chan ST, Stevens DE, Lee RL (2000) A model for flow and dispersion around buildings and its validation using laboratory measurements. US Department of Energy, Report UCRL-JC-137458
12. Al-Khalidy N (2006) Computational fluid dynamics simulation of turbulent flows and pollutant dispersions around groups of buildings. VIPAC Engineers, Report
13. Watkins S, Milbank J, Loxton B (2006) Atmospheric winds and their effects on micro air vehicles. AIAA J 44:2591–2600
14. Watkins S, Fisher A, Mohamed A, Marino M, Thompson M, Clothier R, Ravi S (2013) The turbulent flight environment close to the ground and its' effects on fixed and flapping wings at low Reynolds number. In: 5th European conference for aeronautics and space sciences
15. Mccarley JS, Wickens CD (2004) Human factors concerns in UAV flight. University of Illinois at Urbana-Champaign Institute of Aviation, Aviation Human Factors Division, Savoy
16. Sprater A (1914) Stabilizing device for flying machines. 1119324, US Patent Office, Alexandria, VA
17. Harpur NF (1973) Effect of active control systems on structural design criteria. Advisory Group for Aerospace Research and Development, AGARD, Washington
18. Hawk J, Connor RJ, Levy C (1952) Dynamic analysis of the C-47 gust load alleviation system. SM 14456, Douglas Aircraft, Santa Monica, CA
19. Kraft CC (1956) Initial results of a flight investigation of a gust alleviation system, TM-3612. NASA, Washington, DC
20. McLean D (1978) Gust-alleviation control systems for aircraft. In: Proceedings of the institution of electrical engineers—control and science. IEE, Loughborough, 125
21. Mohamed A, Clothier R, Watkins S, Sabatini R, Abdulrahim M (2014) Fixed-wing MAV attitude stability in atmospheric turbulence. Part 1: suitability of conventional sensors. Prog Aerosp Sci 70:69–82
22. Mohamed A, Clothier R, Watkins S, Sabatini R, Abdulrahim R (2014) Fixed-wing MAV attitude stability in atmospheric turbulence. Part 2: investigating biologically-inspired sensors. Prog Aerosp Sci 71:1–13
23. Ren J, Fu W, Yan J (2018) Gust perturbation alleviation control of small unmanned aerial vehicle based on pressure sensor. Int J Aerosp Eng
24. Blower CJ, Wickenheiser AM (2010) Biomimetic feather structures for localized flow control and gust alleviation on aircraft wings. In: 21st International conference on adaptive structures and technologies. State College, PA
25. Barron Associates. Adaptive control for synthetic jet actuators. https://www.barron-associates.com/adaptive-control-of-synthetic-jet-actuators/. Assessed 15 Aug 2018
26. Tropea C, Yarin AL, Foss JF (2007) Springer handbook of experimental fluid mechanics, vol 1. Springer, Berlin
27. Cheung P, Lam CC, Chan PW (2008) Estimating turbulence intensity along flight paths in terrain disrupted airflow using anemometer and wind profiler data. In: Proceedings of conference of mountain meteorology, Report P2.29
28. Tilmann CP, Langan KJ, Betterton JG, Wilson MJ (2000) Characterization of pulsed vortex generator jets for active flow control. In: Proceedings of RTO AVT, Report RTO MP-051
29. Moore N (2008) Birds, bats and insects hold secrets for aerospace engineers. http://ns.mich.edu/htdocs/releases/story.php?id=6312. Assessed 28 Aug 2018
30. Send W et al (2012) Artifcial hinged-wing bird with active torsion and partially linear kinematics. In: 28th International congress of the aeronautical sciences, 2012
31. Dubois G (2018) Modeling and simulation. CRC Press, Boca Raton
32. Karnopp DC, Margolis DL, Rosenberg RC (2000) System dynamics modeling and simulation of mechatronic systems. Wiley, Canada
33. Pourtakdoust SH, Karimain Aliabadi S (2012) Evaluation of flapping wing propulsion based on a new experimentally validated aeroelastic model. Scientia Iranica B 19(3):472–482
34. Xu M, Wei M, Yang T, Lee YS, Burton TD (2011) Nonlinear structural response in flexible flapping wings with different density ratio. In: 49th AIAA aerospace sciences meeting including the New Horizons forum and aerospace exposition, AIAA 2011–376
35. Mukherjee I, Omkar SN (2011) An analytical model for the aeroelasticity of insect flapping. In: 52nd AIAA/ASME/ASCE/AHS/ASC structures, structural dynamics and materials conference. AIAA, pp 2011–2012
36. Beards CE (1996) Structural vibration: analysis and damping. Arnold, a member of the Hodder Headline Group, Britain
37. Jahanbin Z, Ghafari AS, Ebrahimi A, Meghdari A (2016) Multibody simulation of a flapping-wing robot using an efficient dynamical model. J Braz Soc Mech Sci Eng 38(1):133–149
38. Daniel T, Combes S (2002) Flexing wings and fins: bending by inertial or fluid dynamic forces. Int Comput Biol 42:1044–1049
39. Combes SA, Daniel TL (2003) Into thin air: contributions of aerodynamic and inertial-elastic forces to wing bending in the hawk moth manduca sexta. Exp Biol 206:2999–3006
40. Chin DD, Lentink D (2016) Flapping wing aerodynamics: from insects to vertebrates. J Exp Biol 219(7):920–932

41. Communier D, Salinas MF, Moyao OC, Botez RM (2015) Aero structural modeling of a wing using CATIA V5 and XFLR5 software and experimental validation using the Price- Païdoussis wing tunnel. In: AIAA atmospheric flight mechanics conference, AIAA AVIATION forum. AIAA, pp 2015–2558
42. Abbasi SH, Mahmood A (2019) Modeling, simulation and control of a bio-inspired electromechanical feather for gust mitigation in flapping wing UAV. In: 2nd International conference on communication, computing and digital systems (C-CODE' 19), Pakistan